Int. J. Electrochem. Sci., 11 **(2016)** 10498 – 10510, doi: 10.20964/2016.12.76

International Journal of
ELECTROCHEMICAL
SCIENCE
www.electrochemsci.org

Short Communication

The Transformation of Corrosion Products on Weathering Steel by Visible-Light Illumination under Simulated Marine Atmospheric Condition

Ping Qiu[*], *Zeshun Chen, Hongfei Yang, Lianjie Yang, Li Luo, Changfeng Chen*

Beijing Key Laboratory of Failure, Corrosion and Protection of Oil/gas Facilities and department of Materials Science and Engineering, China University of Petroleum, Beijing 102249, China
[*]E-mail: qiuping@cup.edu.cn

Received: 17 August 2016 / *Accepted:* 13 October 2016 / *Published:* 10 November 2016

This study has explored the visible-light illumination promoted corrosion behavior of weathering steel in simulated marine atmospheric condition. Open circuit potential measurements supplied a direct insight on this photovoltaic effect. To obtain better understanding on this process, the corresponding surface electronic properties together with its microstructures and chemical composition variations were characterized by Mott-Schottky analysis, AFM, XPS and confocal Raman microspectroscopy. All these combined results revealed that the rusted weathering steel sample collected in the dark displayed n-type photo-response due to the presence of hematite (α-Fe_2O_3), maghemite (γ- Fe_2O_3), lepidocrocite (γ-FeOOH) and goethite (α-FeOOH) on its surface. Whereas under illumination, the photogenerated electron-hole pair not only facilitated anodic dissolution and chloride ion adsorption but also leading to hematite to magnetite (Fe_3O_4) transformation in the metal/corrosion layer interface.

Keywords: Atmospheric corrosion; Corrosion products; Visible-light illumination

1. INTRODUCTION

The exploitation of marine oil and gas resources plays an important role on ensuring global petroleum supplies in current situation. As the marine infrastructures developing, a large number of weathering steel are applied in marine atmospheric condition. The corresponding corrosion problem is the major causes of these equipment failures. Many investigations have studied the corrosion behavior induced by polluted gases and aggressive ions [1-6]. Since strong sunlight is one of the marine environmental factors. Some studies have considered solar illumination as a heat source to promote the corrosion process by inducing metal surface wet-dry cycling [1, 7]. Besides, there is also clear

evidence for the photosensitivity of the atmospheric corrosion process in earlier study by Graedel et al. [8]. Burleigh studied the photo-corrosion of different metal during long-term exposure to UV light and proposed a zinc surface dissolution model based on the measured positive photo-voltage [9]. Chen reported the effect of UV illumination on the sodium chloride-induced atmospheric corrosion of pure zinc and weathering steel. They emphasized the relationship between semiconductor properties of the corrosion products and photovoltaic effect [10, 11]. Moreover, the combined influence of UV illumination with contaminants including carbon dioxide and ozone on silver sample were also intensively studied qualitatively and quantitatively [12-14]. The photoactive behavior of anodic passivated films formed on iron or steel surface were widely characterized in even earlier studies [15-18].

Although some studies have presented the effect of UV illumination on the atmospheric corrosion of metals, the initial corrosion behavior and mechanism of weathering steel in marine atmospheric condition under illumination is still not fully understood. What's more, visible light shares about 43% of the whole sunlight spectrum, which matches most iron oxides and hydroxides band gap energy [9, 10]. Accordingly, there are strongly requirements on exploring its influence on the atmospheric corrosion of weathering steel.

In this study, visible-light illumination induced initial corrosion behavior of weathering steel was determined by electrochemical tests. To further disclose the corresponding corrosion mechanism, the corrosion products microstructures and chemical compositions variations were also characterized.

2. EXPERIMENTAL

2.1 Materials and sample preparation

Weathering steel foil (carbon: 0.05, silicon: 0.30, manganese: 0.81, copper: 0.33, nickel: 0.12, chromium: 0.70, phosphorous: 0.01, sulphur: 0.005 wt %) is the object investigated in this study. Each foil, dimension of 1 cm^2, was abraded with silicon carbide paper to 2000 mesh. Samples prepared for AFM analysis were further polished with a diamond paste down to 0.5 μm. Finally, all samples were ultrasonically cleaned in ethanol for 5 min, flushed with nitrogen, and then transferred into desiccator.

Sodium chloride particles were deposited on each sample surface before exposure. This was achieved by saturating sodium chloride particles in ethanol. Then small quantities of the solution were deposited on polished sample surface by a transfer pipette. Evenly distributed Sodium chloride particles were obtained after ethanol volatilized. The resulting concentration of sodium chloride deposited on each sample surface is 4 $\mu g/cm^2$.

Powders of commercial hematite and magnetite with high spectral purity (Sigma-Aldrich) were used as received for phase spectrum studies.

2.2 Exposure condition

The laboratory exposure apparatus was similar to the one used in previous work [19]. A light shielded exposure chamber with the diameter of 20 cm and the height of 30 cm was used, which was

set at a thermal bath to keep constant temperature. Top lid of the chamber was fixed by quartz window to supply the maximum visible-light transmission. The light source was a 500 W xenon lamp with UV cutoff filter (providing visible light $\lambda \geq 420$ nm). Compressed and purified dry air was used as flow air and divided into two parts. One part passed through a distilled water bottle to produce humidified air. Then by mixing the humidified air with the other part of the dry air, the desired mixed air passed through the exposure chamber with the velocity of 50 ml/min as controlled by air flow meter. The relative humidity and temperature were continuously monitored by temperature/humidity sensor at the outlet of the mixed air. The incident heat effect was monitored during the exposure, the resulting temperature fluctuation was less than 1℃, which has no essential influence on corrosion process. So each exposure was performed on the sodium chloride pre-deposited sample at $95\pm3\%$ RH with a constant temperature of 25 ± 1℃ in the dark or under visible-light illumination for 3 days. Triplicate weathering steel foils were exposed under each exposure condition.

After exposure in this mild accelerated condition, a thin corrosion product layer is formed on weathering steel surface, which is mainly composed of iron oxides and iron hydroxides. Earlier studies indicated that the withdraw sample is suitable for the following electrochemical tests and surface analysis [11, 20].

2.3 Electrochemical measurements

In order to explore the light induced electrochemical process changes on the rusted surface, electrochemical tests were selectively performed with a Zahner IM6eX station equipped with LED lamp (visible light $\lambda \geq 420$ nm). A quartz window in diameter of 3 cm was fitted to the front of the electrochemical cell. The other parts of the cell were intentionally shielded with room light. A standard three-electrode system was used with a saturated calomel electrode (SCE) as the reference electrode, platinum wire as the counter electrode and the rusted weathering steel samples after laboratory exposure as the working electrode. The exposed sample surface area was 1 cm^2. All electrochemical tests were conducted in naturally aerated 1 wt. % sodium chloride solution. Triplicate rusted samples were used for each test. The corresponding representative results were reported.

Illumination induced open circuit potential (OCP) variations of the rusted sample were monitored under intermittent visible light on and off. Polarization curves were obtained from -0.12 V to 0.12 V (vs. OCP) at the scan rate of 1 mV/s. Mott-Schottky plots were measured by applying an AC voltage magnitude of 5 mV with the frequency of 1KHz. The scanned potential was set in the range of -0.50 V to -0.20V.

The phase spectra test system included a source of monochromatic light, a lock-in amplifier (SR830, Stanford research system, inc.) with a light chopper (SR540, Stanford research system, Inc.) and a photovoltaic cell. A 500 w xenon lamp and a grating monochromator (Omni-5007, No.09010, Zolix) were combined to produce the monochromatic light. The chopping frequency was set as 24 Hz. The samples including hematite pellet and bi-layer magnetite/hematite pellet were arranged between the back electrode and the indium tin oxide (ITO) electrode. The back electrode was connected to the common grounding point of the lock-in-amplifier.

2.4 Surface characterization

The rusted weathering steel surface microstructures and chemical composition variations were further characterized to help in revealing the corresponding corrosion mechanism.

The surface topography of rusted weathering steel was studied by atomic force microscopy (AFM, MultiMode 3D SPM System, Bruker Corporation). The applied probe was antimony doped n-type silicon tip with a spring constant of 40 N/m and resonant frequency of 300 KHz. All measurements were performed in contact mode. The scan rate was 1 Hz.

X-ray photoelectron spectroscopy (XPS) was applied to investigate the chemical composition of the outermost surface layer of the rusted sample. PHI Quantera XPS system was selected for both wide and detailed scans of Fe 2p and O 1s using a monochromic aluminium Ka X-ray source (1486.6 eV) operated at 25 W (15kV/1.7 mA) with the chamber vacuum at 1.33 μPa.

Confocal Raman microspectroscopy measurements were performed with a HORIBAHR-800 system equipped with a laser source of wavelength 514 nm. The spectral resolution was 1-2 cm^{-1}.

All analyses were conducted at three different surface areas of each rusted sample. Triplicate specimens were tested and the representative results were displayed.

3. RESULTS AND DISCUSSION

3.1 Characterization of corrosion products

As known, the rusted metal surface state play an important role on its corrosion behavior. So this section will present the influence of visible-light illumination on the weathering steel surface microstructures and chemical compositions.

Firstly, AFM measurements were performed on the rusted surface of weathering steel after 3 days exposure in the dark or under illumination.

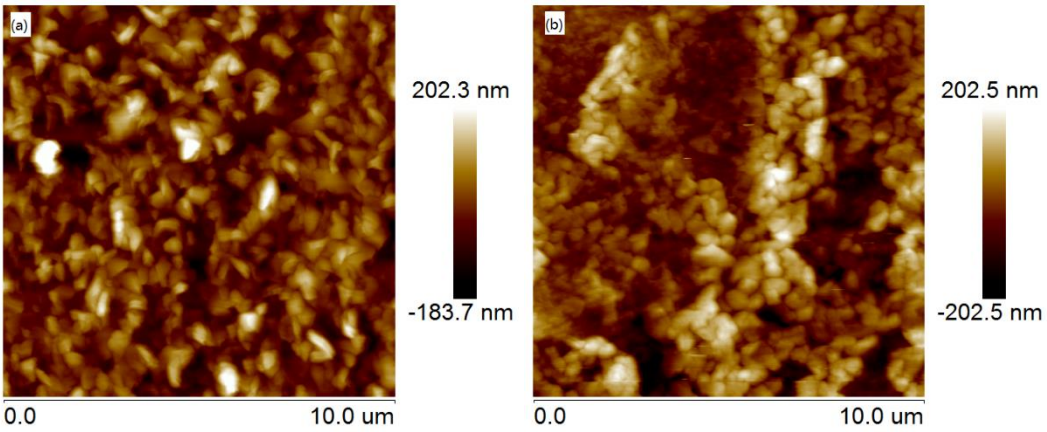

Figure 1. AFM images of the corrosion products formed on weathering steel surface after 3 days exposure in the dark (a) or under visible-light illumination (b) in humid air at 25 ℃, 95% RH.

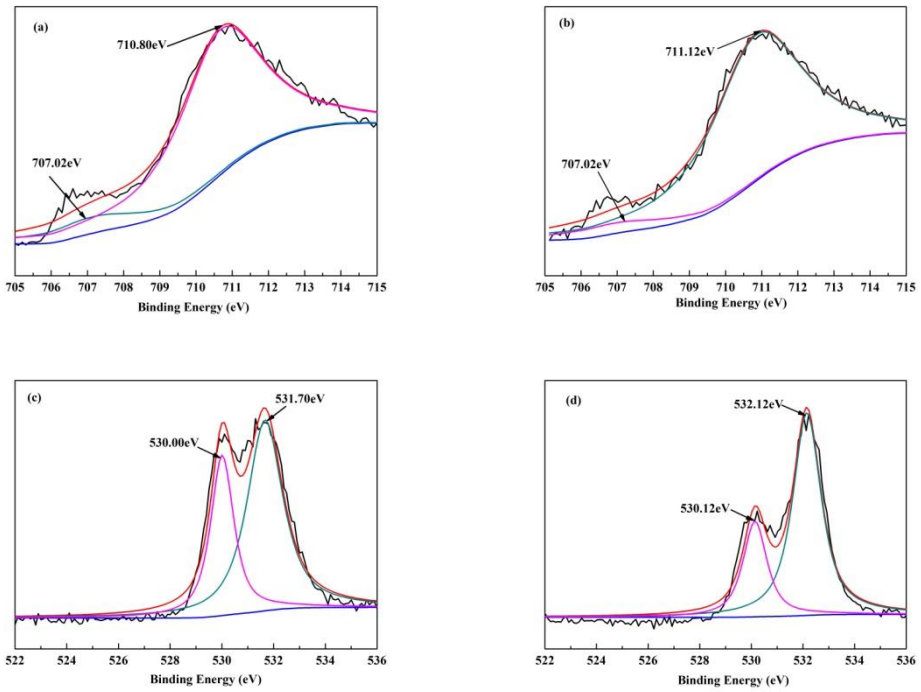

Figure 2. XPS spectra of the corrosion products formed on weathering steel surface after 3 days exposure under visible-light illumination in humid air at 25 ℃, 95% RH. (a) Fe 2p in the dark, (b) Fe 2p under illumination, (c) O 1s in dark condition, (d) O 1s

The corrosion products formed in the dark present small feather-like features (Fig.1 (a)). In comparison, the corrosion products are porous rod-like under illumination (Fig.1 (b)). The relative height fluctuation of the corrosion products is much remarkable than in the dark condition. So AFM results indicate that visible-light illumination could apparently effect the surface topography variations, which imply a potential influence on the corresponding corrosion process.

Average compositional analysis by XPS can help to determine the main corrosion products composition in the outermost surface of the rusted sample. Fig. 2 (a) presents the XPS spectrum of Fe 2p collected on the sample after 3 days exposure in dark condition. The peak at 707.2 eV and 711.2 eV could be ascribed to metallic iron and iron (III) respectively [21]. Furthermore, the XPS spectrum of O 1s was obtained on the same sample (Fig. 2 (c)), where the 530.00 eV peak corresponds to the lattice oxygen atom in hematite (α-Fe_2O_3) and the 531.1 eV peak corresponds to the water/hydroxide group [21]. Based on above analysis, hematite/ferric oxyhydroxide could be determined as the main corrosion products in the outer layer of the rusted sample surface exposed in dark condition. Fig. 2 (b) and (d) display XPS spectra collected on the rusted sample after 3 days exposure under illumination. Although similar peaks are assigned, both the binding energy of Fe2p peak and O1s peak slightly shift to higher energy level comparing to Fig. 2(a) and (b). It might imply a crystal structure transformation between hematite and maghemite (γ-Fe_2O_3) [22].

XPS is capable of revealing outer surface layer chemical state, as a complementary tool, confocal Raman spectroscopy is selected to detect the bulk corrosion products composition. Fig. 3

shows the Raman spectra of the corrosion products formed on weathering steel after 3 days exposure in the dark or under illumination. The bands corresponding to lepidocrocite (γ-FeOOH) and goethite (α-FeOOH) observed in both Raman spectra [23]. Besides, the main corrosion products formed on weathering steel in dark condition are hematite and maghemite. However, the corrosion products are mainly presented as hematite and magnetite (Fe_3O_4) after illumination. Furthermore, the main sharp band appeared at ～673 cm^{-1} together with the shoulder at ～630 cm^{-1} are also suggested as spinel structure solid solution of ferric chromium oxide ($Fe_{1.8}Cr_{1.2}O_4$) [24].

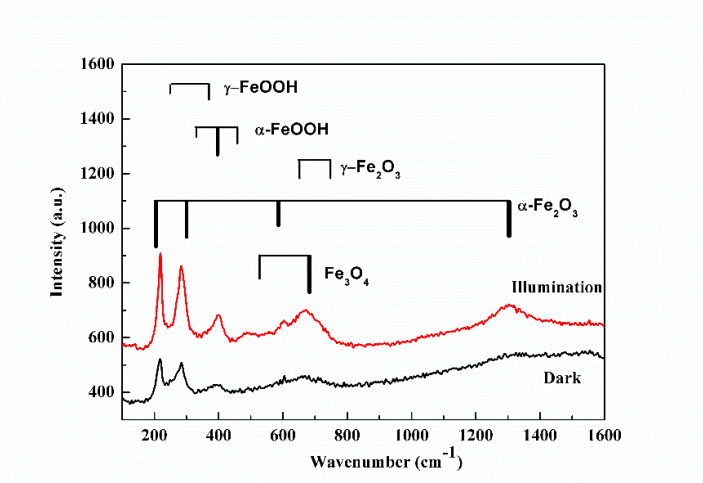

Figure 3. Raman spectra of the corrosion products formed on weathering steel surface after 3 days exposure in the dark or under visible-light illumination in humid air at 25 ℃, 95% RH.

Importantly, the presence of magnetite by Raman observation instead of XPS analysis may imply a bi-layer structure of the corrosion products formed under illumination: inner layer magnetite mixed with ferric chromium oxide and outer layer of hematite/ferric oxyhydroxide. In addition, this bi-layer structure has been mentioned in some works that the inner presence of magnetite layer was due to limitation of oxygen supply [23, 25, 26]. As far as the literatures we know, it is the first time been found that visible-light illumination could facilitate this process.

3.2 Light induced electrochemical process variations

The above surface analysis results have provided substantial evidences on visible-light illumination induced corrosion layer microstructures and chemical compositions variations. However, corrosion is an essentially electrochemical process in current condition. A deep understanding of the corrosion behavior should be based on electrochemical tests. So visible-light illumination induced OCP changes were monitored in 1 wt.% sodium chloride solution on the rusted weathering steel sample after 3 days exposure in the dark, displayed in Fig. 4. It can be seen that the illumination arouses a positive photo-voltage on the rusted sample by increasing the OCP for about 10 mV. As XPS and Raman results revealed, the corrosion products formed on rusted sample include mainly hematite/ferric oxyhydroxide in the dark, which are n-type semiconductors and active to visible-light

illumination [27, 28]. So the absorption of photons on corrosion products surface can create electron hole pair. The resulting positive potential shift suggested that the photogenerated holes move to the inner layer, however, the corresponding electrons migrate towards the outer layer. This photo-active behaviour is consistence with others observation performed on the atmospheric corrosion of zinc and weathering steel under UV illumination [9-11].

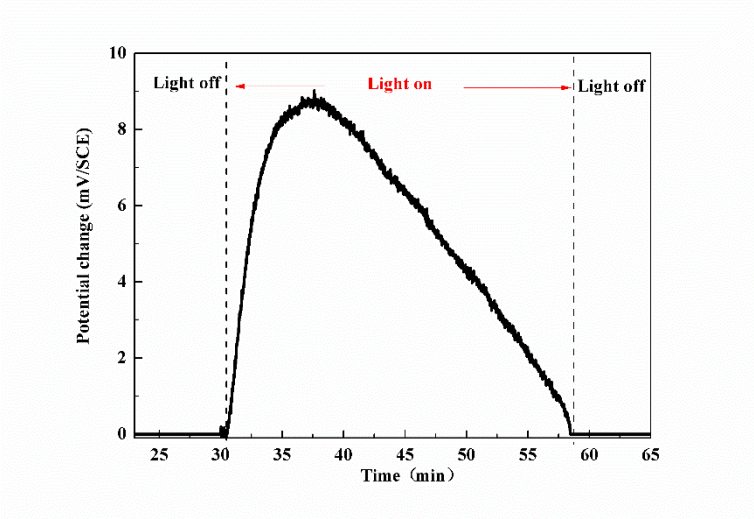

Figure 4. Representative open circuit potential variations recorded in naturally aerated 1 wt.% sodium chloride solution under intermittent visible light on and off for weathering steel after 3 days exposure under dark condition in humid air at 25 ℃, 95% RH.

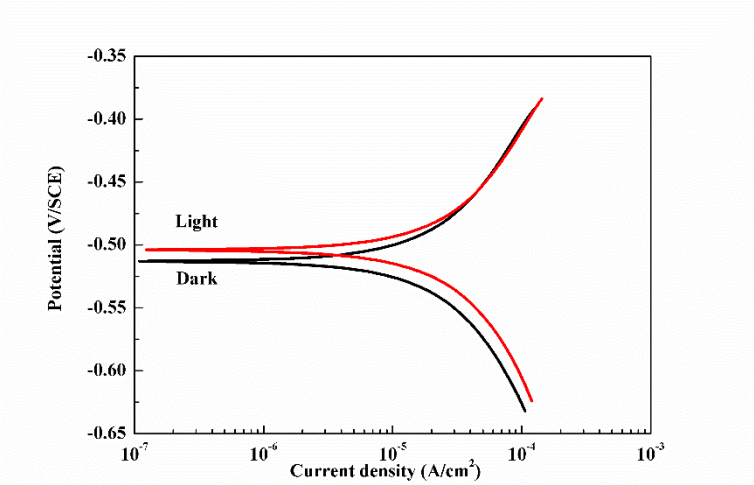

Figure 5. Comparison of representative polarization curves recorded at the scan rate of 1 mV/s in naturally aerated 1 wt.% sodium chloride solution for weathering steel after 3 days exposure in the dark or under visible-light illumination in humid air at 25 ℃, 95% RH.

Since the rusted weathering steel presented photovoltaic effect, the influence of visible-light illumination on its corrosion kinetics is worth to be studied. Potentiodynamic polarization curves for the rusted weathering steel samples after 3 days exposure in the dark or under illumination are recorded in 1 wt.% sodium chloride solution, shown in Fig. 5. Within the scanned potential range,

there is no obvious reduction or oxidation process observed. Both plots show good linear relationships in the higher potential region. The anodic and cathodic curves are extrapolated up to their intersection where corrosion current density (i_{corr}) and corrosion potential (E_{corr}) are obtained and listed in Table 1.

It can be seen that the i_{corr} value of the rusted sample after 3 days exposure under illumination increases about 24% than that of in the dark. Therefore, it confirms that visible-light illumination greatly accelerate the weathering steel corrosion process.

Table 1. Electrochemical kinetic parameters associated with polarization curves recorded at the scan rate of 1 mV/s in naturally aerated 1 wt.% sodium chloride solution for weathering steel after 3 days exposure in the dark or under visible-light illumination in humid air at 25 ℃, 95% RH.

.

Sample	E_{corr} [V/SCE]	i_{corr} [μA/cm^2]	β_a [V/decade]	$-\beta_c$ [V/decade]
Dark	-0.513	19.741	0.151	0.152
Illumination	-0.504	24.529	0.150	0.160

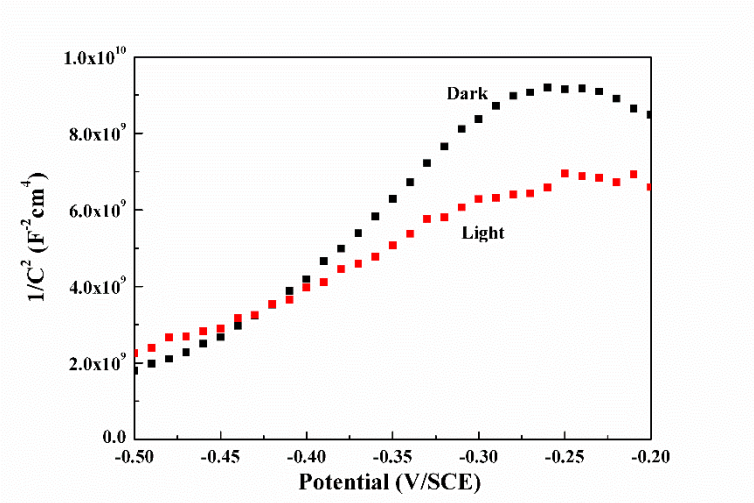

Figure 6. Comparison of Mott-Schottky plots recorded with 5 mV AC voltage at 1KHz for the weathering steel after 3 days exposure in the dark or visible-light illumination in humid air at 25 ℃, 95% RH.

Subsequently, the electronic properties of the corrosion products formed on the weathering steel after 3 days exposure in the dark or under illumination were explored by impedance method. The representative Mott-Schottky plots are presented in Fig. 6. Judging from the slope in the linear part of the plots, they present positive values. So the corrosion products formed in both conditions are similar

to n-type semiconductors. This is agree with generally view on electronic property of the corrosion products formed on steel [11, 25].

For an n-type semiconductor, the relationship between applied potential and capacitance of the space charge region is as follows [29, 30]:

$$\frac{1}{C_{sc}^2} = \frac{2}{\varepsilon\varepsilon_0 qN_D}(E - E_{FB} - \frac{kT}{q}) \qquad (1)$$

Where C_{sc} is the capacitance of the space charge region in the semiconductor; ε is the relative permittivity of the semiconductor, here the value of 10 is adopted from similar studies [31-33]; ε_0 is the permittivity in vacuum (8.85×10^{-14} F·cm^{-1}); q is the charge of the electron (1.602×10^{-19} C); N_D is the charge carrier density (charge carries·cm^{-3}); E is the applied potential (V); E_{FB} is the flatband potential (V); KT/q is known as 25mV at room temperature.

So the charge carrier density (N_D) and flatband potential (E_{FB}) can be calculated from the plots presented in Fig. 6. The N_D values is 4.5×10^{20} cm^{-3} for the sample exposed under illumination, which is higher than that of the corrosion products formed in the dark, 2.2×10^{20} cm^{-3}. This suggested that the visible-light illumination increased the electric conductivity and oxygen vacancy of the corrosion products [32, 34]. This may ascribed to magnetite formation on the rusted sample exposed under illumination (shown in Fig.3), which presents rather narrow band gap energy and higher oxygen vacancies comparing with hematite and ferric oxyhydroxide (the main corrosion products formed on the rusted sample exposed in the dark) [35].

Furthermore, the value of E_{FB} is -0.41V and -0.53 V for the rusted sample exposed in the dark and illumination respectively. It is evident that the E_{FB} shift to the negative potential. It is attributed to the even more chrolide ions migrations to the inner corrosion products formed on weathering steel exposed under illumination than in the dark.

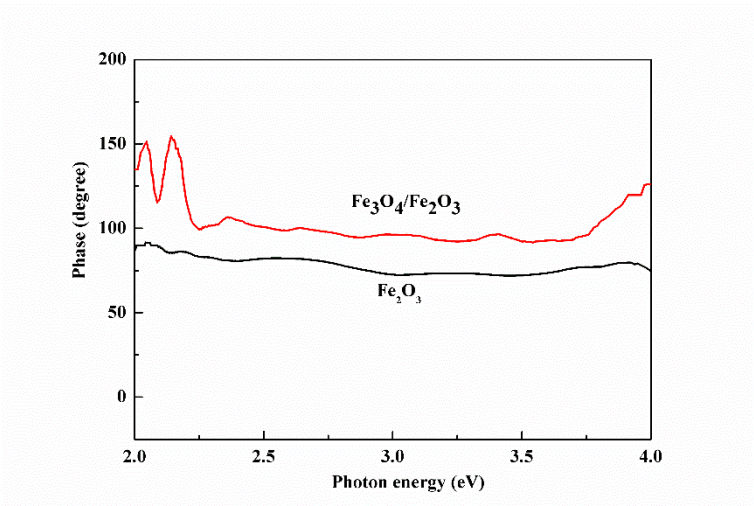

Figure 7. Surface photovoltage phase spectra recorded on pure Fe_2O_3 and Fe_3O_4/Fe_2O_3 bi-layer pellet.

Since XPS and Raman spectroscopy analysis results implied a bi-layer structure of the corrosion products formed under light illumination: inner layer magnetite mixed with ferric chromium oxide and outer layer of hematite/ferric oxyhydroxide. In order to disclose this structure validity, the

SPV measurement was carried out. Fig. 7 displays the phase spectra obtained on pure hematite pellet and magnetite / hematite bi-layer pellet, which simulate the main corrosion products formed on weathering steel after exposure in the dark and under illumination respectively. It can be seen that the phase values are below 90^o for pure hematite sample and are above 110^o for magnetite / hematite bi-layer pellet. Others studies have suggested that the response of phase value in the second quadrant indicated the migration of photogenerated electrons towards the outer layer of the pellet [27, 36]. This is consistence with our OCP observations (Fig. 4). On the other hand, this consistence also confirm that the bi-layer pellet structure to mimic the corrosion products formed on weathering steel under illumination is reasonable.

3.3 Modeling of light induced corrosion process variations

The above combined analyses revealed the photo-active behavior of the corrosion products formed on weathering steel in simulated marine atmospheric condition. A model is proposed to illustrate the interaction between photons and the corrosion products, as shown in Fig. 8.

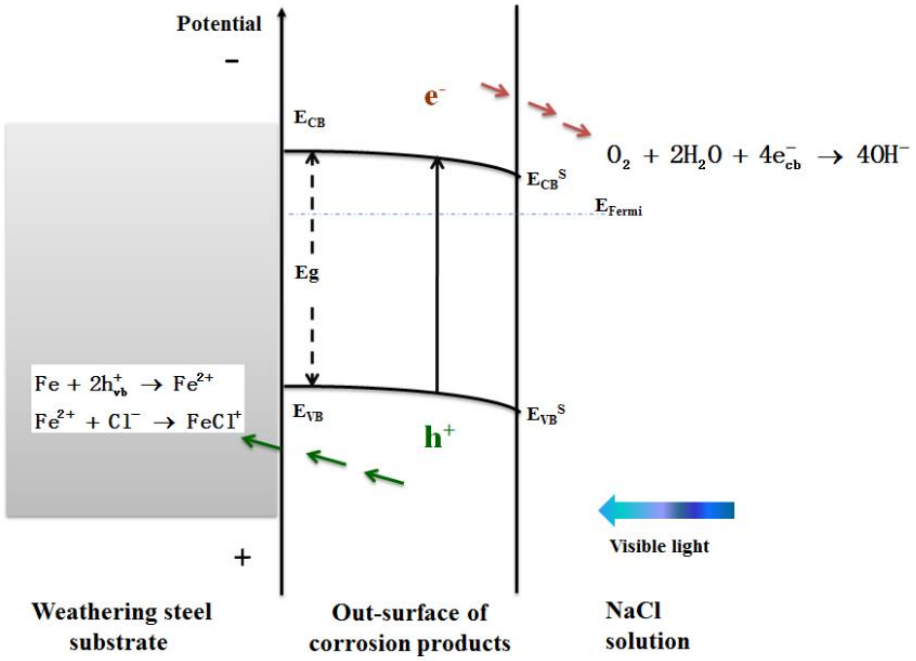

Figure 8. Schematic illustration of the band energy and the charge transfer process in the corrosion product layer formed on weathering steel specimen exposed to the humid air at room temperature under visible-light illumination.

Firstly, the main corrosion products are mixture of hematite and ferric oxyhydroxide on weathering steel after exposed in dark condition (Fig. 2 and 3). These corrosion products are highly doped n-type oxides (Fig. 6). The location of the Fermi level, CB potential and VB potential of the corrosion products are illustrated in Fig. 8. Since the corrosion products Fermi level is more negative

than that of oxygen / water (+1.229 V vs. SHE), a new Fermi level is built between the corrosion products and the exposure media to compensate the Fermi level difference [11]. So the energy band at the interface bends downward, a space charge layer is built. The band gap energy of hematite / ferric oxyhydroxide is between 2.2-2.6 eV, which can absorb the light wavenumber lower than 564 nm [27, 37]. When visible light illuminate the corrosion products, photogenerated electron-hole pairs are created. According to the energy bending in the space charge layer, the electrons in the CB flow downward to the exposure media and the corresponding holes in the VB migrate to the weathering substrate. Consequently, a positive photo-voltage is observed in OCP measurements.

The process can be described as following:

$$Fe_2O_3/FeOOH + hv \rightarrow e_{cb}^- + h_{vb}^+ \quad (2)$$

The photogenerated electrons present strong reducibility, which can accelerate the oxygen reduction, as shown in equation (3). Subsequently, hematite / ferric oxyhydroxide accumulated at the interface. With the corrosion product layer thickness increasing, the diffusion of oxygen to the inner layer is hindered. So iron will oxidise incompletely and form magnetite. Continuously, a duplex oxide film forms composed by an inner Fe_3O_4 layer and a thick outer hematite / ferric oxyhydroxide scale. Furthermore, the photogenerated holes can participate in anodic reaction by capturing the electrons from anodic dissolution which can attract the chrolide ion in the exposure media, as presented in the equation (4) and (5).

$$O_2 + 2H_2O + 4e_{cb}^- \rightarrow 4OH^- \quad (3)$$

$$Fe + 2h_{vb}^+ \rightarrow Fe^{2+} \quad (4)$$

$$Fe^{2+} + Cl^- \rightarrow FeCl^+ \quad (5)$$

So all these results revealed that the photogenerated electron-hole pairs can participate in the corrosion process by promoting anodic dissolution and triggering the transformation of hematite / ferric oxyhydroxide (main corrosion products formed on weathering steel after exposed in dark condition) partly to magnetite (that of formed under illumination).

4. CONCLUSIONS

This study has explored the photo-active behavior of corrosion products formed on weathering steel in simulated marine atmospheric condition.

Electrochemical tests have revealed that the visible-light illumination could accelerate the weathering steel surface corrosion rates. The observed positive voltage shifts and the capacitance dependence have clearly demonstrated the photo-active effect and electronic properties of the corrosion products.

The supplements of surface characterizations further confirmed that the corrosion products formed on weathering steel surface presented photovoltaic effect. The related photogenerated electron-hole pairs can participate in the corrosion process by promoting anodic dissolution and triggering the transformation of hematite / ferric oxyhydroxide partly to magnetite.

ACKNOWLEDGEMENTS
This work was supported by the National Natural Science Foundation of China (Grant No. 51301199) and the funding of China University of Petroleum (Beijing) (Grant No. YJRC-2013-45). We are also grateful to the reviewers for the helpful comments.

References

1. L. Hao, S. Zhang, J. Dong, W. Ke, *Corros. Sci*., 58 (2012) 175.
2. L. Hao, S. Zhang, J. Dong, W. Ke, *Corros. Sci.*, 59 (2012) 270.
3. Z. Wang, J. Liu, L. Wu, R. Han, Y. Sun, *Corros. Sci*., 67 (2013) 1.
4. S. Oesch, *Corros. Sci.*, 38 (1996) 1357.
5. M. Yamashita, H. Miyuki, Y. Matsuda, H. Nagano, T. Misawa, *Corros. Sci.*, 36 (1994) 283.
6. T. Misawa, K. Asami, K. Hashimoto, S. Shimodaira, *Corros. Sci*., 14 (1974) 279.
7. S. Hœrlé, F. Mazaudier, P. Dillmann, G. Santarini, *Corros. Sci*., 46 (2004) 1431.
8. T.E. Graedel, J.P. Franey, G.W. Kammlott, *Science*, 224 (1984) 599.
9. T.D. Burleigh, C. Ruhe, J. Forsyth, *Corrosion*, 59 (2003) 774.
10. S. Song, Z. Chen, *J. Electrochem. Soc*., 161 (2014) C288.
11. L. Song, X. Ma, Z. Chen, B. Hou, *Corros. Sci.*, 87 (2014) 427.
12. R. Wiesinger, C. Kleber, J. Frank, M. Schreiner, *Appl. Spectrosc*., 63 (2009) 465.
13. Z.Y. Chen, D. Liang, G. Ma, G.S. Frankel, H.C. Allen, R.G. Kelly, *Corrosion Engineering, Science and Technology*, 45 (2010) 169.
14. D. Liang, H.C. Allen, G.S. Frankel, Z.Y. Chen, R.G. Kelly, Y. Wu, B.E. Wyslouzil, *J. Electrochem. Soc*., 157 (2010) C146.
15. U. Stimming, *Electrochim. Acta*, 31 (1986) 415.
16. P.C. Searson, R.M. Latanision, U. Stimming, *J. Electrochem. Soc.*, 135 (1988) 1358.
17. P. Schmuki, H. Böhni, *Electrochim. Acta*, 40 (1995) 775.
18. J.S. Kim, E.A. Cho, H.S. Kwon, *Corros. Sci*., 43 (2001) 1403.
19. P. Qiu, Quantified In Situ Analysis of Initial Atmospheric Corrosion, in: Chemical Science and Engineering, Royal Institute of Technology (KTH), Stockholm, 2011.
20. P. Kalinauskas, I. Valsiūnas, M. Samulevičien≒, E. Juzeliūnas, *Corros. Sci.*, 43 (2001) 2083-2092.
21. M. Omran, T. Fabritius, A.M. Elmahdy, N.A. Abdel-Khalek, M. El-Aref, A.E.-H. Elmanawi, *Appl. Surf. Sci.*, 345 (2015) 127.
22. A.P. Grosvenor, B.A. Kobe, M.C. Biesinger, N.S. McIntyre, *Surf. Interface Anal.*, 36 (2004) 1564.
23. X. Zhang, K. Xiao, C. Dong, J. Wu, X. Li, Y. Huang, *Engineering Failure Analysis*, 18 (2011) 1981.
24. M. Ortiz Morales, C. Frausto Reyes, J.J. Soto Bernal, S.E. Acosta Ortiz, R. Gonzalez Mota, I. Rosales Candelas, *Spectrochim. Acta, Part* A, 128 (2014) 681.
25. J. Wielant, V. Goossens, R. Hausbrand, H. Terryn, *Electrochim. Acta*, 52 (2007) 7617.
26. Y.H. Huang, T.C. Zhang, *Water Res.*, 39 (2005) 1751.
27. X. Wei, T. Xie, L. Peng, W. Fu, J. Chen, Q. Gao, G. Hong, D. Wang, *J. Phys. Chem*. C, 115 (2011) 8637.
28. A. G. Joly, G. Xiong, C. Wang, D. E. McCready, K. M. Beck, W. P. Hess, *Appl. Phys. Lett.*, 90 (2007) 103504.
29. S.R. Morrison, Electrochemistry at Semiconductor and Oxidized Metal Electrodes, Plenum Press, Second printing, New York, 1984.
30. E. Sikora, D.D. Macdonald, *J. Electrochem. Soc.*, 147 (2000) 4087.
31. Y.F. Cheng, J.L. Luo, *Electrochim. Acta*, 44 (1999) 2947.
32. Y.F. Cheng, C. Yang, J.L. Luo, *Thin Solid Films*, 416 (2002) 169.
33. R. Jiang, C. Chen, S. Zheng, *Electrochim. Acta*, 55 (2010) 2498.

34. E. Sikora, J. Sikora, D.D. Macdonald, *Electrochim. Acta*, 41 (1996) 783.
35. R.M. Cornell, U. Schwertmann, The Iron Oxides, second ed., ed., Wiley-VCH, 2003.
36. V. Donchev, K. Kirilov, T. Ivanov, K. Germanova, *Materials Science and Engineering*: B, 129 (2006) 186.
37. S.R. Morrison, Electrochemistry at semiconductor and oxidized metal eletrodes, Plenum, New York, 1980.